Tetrahedron 71 (2015) 4163–4173

Contents lists available at ScienceDirect

Tetrahedron

journal homepage: www.elsevier.com/locate/tet

Dicationic derivatives of dinaphthotetraaza[14]annulene: synthesis, crystal structures and the preliminary evaluation of their DNA binding properties

Alicja Kaźmierska [a], Marlena Gryl [a], Katarzyna Stadnicka [a], Lesław Sieroń [b], Andrzej Eilmes [a], Justyna Nowak [a], Marija Matković [c], Marijana Radić-Stojković [c], Ivo Piantanida [c], Julita Eilmes [a,*]

[a] Faculty of Chemistry, Jagiellonian University, Ingardena 3, 30-060 Kraków, Poland
[b] Institute of General and Ecological Chemistry, Lodz University of Technology, Żeromskiego 116, 90-924 Łódź, Poland
[c] Division of Organic Chemistry and Biochemistry, Ruđer Bošković Institute, Bijenička cesta 54, PO Box 180, HR-10002 Zagreb, Croatia

ARTICLE INFO

Article history:
Received 19 January 2015
Received in revised form 17 April 2015
Accepted 27 April 2015
Available online 1 May 2015

Keywords:
Dinaphthotetraaza[14]annulene
Synthesis
Structure
Spectroscopy
DNA binding

ABSTRACT

Four new water-soluble, fluorescent derivatives of dinaphthotetraaza[14]annulene (DNTAA) have been synthesized varying in the structure, dimensions and spatial arrangements of their *meso* side groups. The products have been carefully characterized by elemental analyses, spectroscopy, crystal structures and quantum-chemical calculations employing DFT methodology. One representative product of the DNTAA series was tested for DNA binding using UV–vis titrations, CD and thermal denaturation experiments. Intercalation of ds-DNA was recognized as a dominant binding mode. In contrast to non-fluorescent phenylene analogues (DBTAA), reported previously, DNTAA derivative showed threefold fluorescence increase upon DNA binding, and offered intriguing new applications as a fluorescent DNA/RNA dye.

1. Introduction

Non-covalent DNA-recognition by synthetic agents has attracted a great deal of attention and occupied a number of research groups because of its relevance in biology and medicine.[1] The most attractive and stimulating reason of the research in this area seems to be the well-established fact that many therapeutic agents, particularly anticancer drugs, interact with nucleic acids via non-covalent binding motifs, such as intercalations between base pairs, minor/major groove binding and outside binding with self-stacking along the DNA skeleton.[2] The search for properly designed molecules able to interact efficiently and selectively with nucleic acids is therefore, still of crucial importance.

We have recently shown in several reports that dibenzotetraaza [14]annulene (DBTAA) macrocycle was useful in the preparation of novel receptors with higher complexity.[3] It was demonstrated, among other results that dicationic DBTAA derivatives may be of value in research aiming at rational design and preparation of DNA binding agents. In particular, the new compounds subjected to our tests appeared to interact with DNA and RNA by mixed minor groove and intercalative binding modes. They further revealed significant antiproliferative activity against human tumour cell lines. It was also shown that non-covalent interactions with DNA and RNA were strongly dependent on steric factors characterizing cationic peripheral substituents. By variation of the dimensions, the rigidity and the exposure of the positive charges in the side groups, we were able to fine-tune their binding properties toward nucleic acids.[4] Most recently, based on the structure of the most active compounds, we have designed and synthesized DBTAA-conjugate bearing adenine in the side group, which appeared able to recognize selectively complementary poly dT among ss-DNA/ss-RNA sequences.[5]

Currently, we have started to modulate the DNA binding properties of our receptors by variation of the size of main macrocyclic unit. In this work we report on the synthesis, crystal structure and preliminary evaluation of the new series of potential DNAbinding agents constructed on the basis of dinaphthotetraaza[14]annulene (DNTAA) skeleton (Fig. 1). Compared with the DBTAA derivatives studied earlier in our group, the molecules of the new compounds contain more extended aromatic system due to incorporation of *o*-naphthylene units in the place of *o*-phenylene groups.

* Corresponding author. Tel.: +48 12 6632294; fax: +48 12 6340515; e-mail address: jeilmes@chemia.uj.edu.pl (J. Eilmes).

http://dx.doi.org/10.1016/j.tet.2015.04.098
0040-4020/

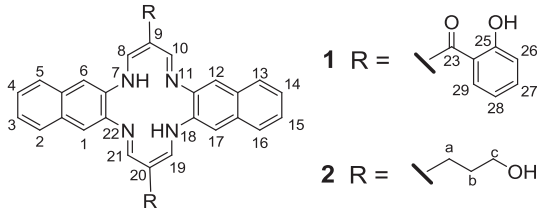

Fig. 1. DNTAA substrates **1** and **2**.

Knowing that molecular recognition relies on geometric matching and that intercalation strength of a ligand in DNA depends mainly on the size of the aromatic moiety[6] we believe that the molecules with larger π-electron systems will exhibit improved binding properties. We hope that strongest affinity of DNTAA-based receptors toward nucleic acids will allow us to more efficiently tune their selectivity.

It also seems of significant importance that due to incorporation of the *o*-naphthylene chromophores in the molecules, DNTAA-based binding agents offer the additional advantage of a built-in fluorescent signal, useful in exploring non-covalent interactions.[7]

For the sake of solubility in water and to increase the affinity to the polyanionic DNA skeleton, the molecules of the new compounds are equipped with positively charged side groups, varying in length, rigidity and bulkiness. The new products represent two types of receptors differing mainly in the structure, dimensions and spatial arrangement of the *meso* peripheral substituents. In the compounds **6**–**8** (Scheme 1), the charged side chains are attached to the main ring through linkers containing rigid *o*-benzoyl moieties. This affects significantly the directional arrangement of the side chains, which are therefore folded below and above the main planar macrocycle. This was shown by single crystal X-ray measurements of the compound **8**.[8]

Dimensions of the molecules and details of the three-dimensional structures of representative new compounds **2**, **8**[8] and **9** are discussed based on X-ray measurement data. Electronic characteristics of the new receptors are evaluated on the basis of UV–vis spectra and quantum-chemical calculations employing DFT methodology.

2. Results and discussion

2.1. Synthesis

The macrocyclic substrate **1** (Fig. 1) was synthesized by the procedure described previously,[8] compound **2** was prepared starting from 2,3-diaminonaphthalene and 3,4-dihydro-2*H*-pyran-5-carbaldehyde, similarly to the reported earlier dibenzotetraaza [14]annulene analogue.[9] Compound **1**, fairly insoluble in organic solvents, was transformed into water-soluble derivatives **6**–**8** via two consecutive alkylations. Thus, the reactions of **1** with 1,3-dibromopropane and 1,4-dibromobutane gave corresponding dibromides **3** and **4**, respectively, which were next used for alkylation of trimethylamine and pyridine. 9,20-Bis(3-hydroxypropyl)-dinaphthotetraaza[14]annulene **2** was transformed to **5** via Appel methodology using PPh_3–CBr_4 mixture.[10] The reaction of **5** with pyridine allowed the isolation of water-soluble dicationic product **9**.

It is worth mentioning here that alkylation of **1** with 1,4-dibromobutane produced dibromide **4**[8] in 22% yield along with a *lacunar* counterpart **10** (Scheme 2), isolated in 14% yield by careful chromatography of the reaction mixture. Relatively easy formation of the by-product **10** points to significant propensity of **1** to be intramolecularly bridged by appropriate bifunctional reagents. Similar tendency to *lacunization* observed by us previously for the corresponding DBTAA analogue was explained in terms of favourable steric exposure of reacting OH centres.[11] The pentamethylene

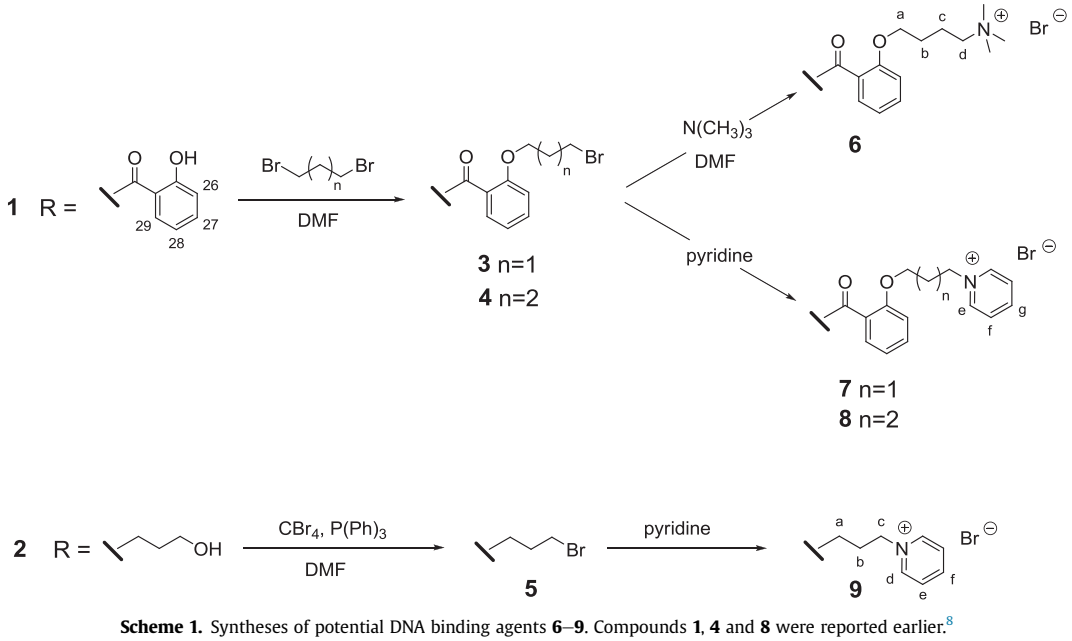

Scheme 1. Syntheses of potential DNA binding agents **6**–**9**. Compounds **1**, **4** and **8** were reported earlier.[8]

In contrast, compound **9** has a less congested structure allowing unhindered access to both faces of the macrocyclic moiety, it therefore seems to be especially well suited for intercalation in DNA. It is equipped with flexible side chains, which freely stretch outside the macrocyclic core.

bridge was then found to be the shortest one able to span distant OH groups in the *o*-phenylene-based substrate.[3d] Here, isolation of **10** suggested that dinaphtho analogue **1** was also perfectly suited for efficient intramolecular bis-alkylation without need of using high-dilution conditions.

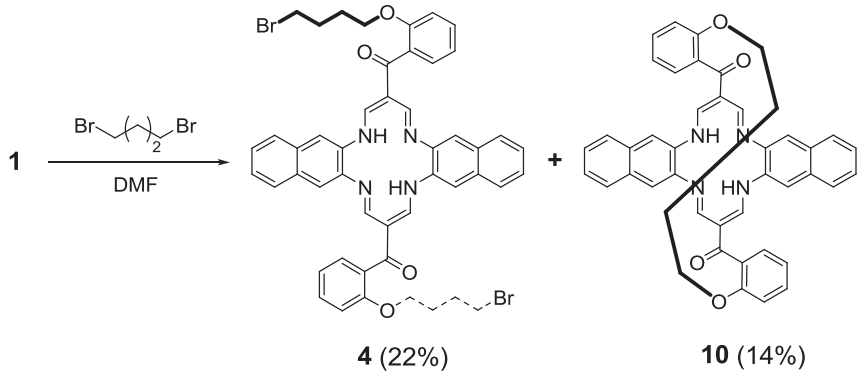

Scheme 2. Synthesis of the lacunar compound **10**.

The characterization of the new products was based on ^{1}H and ^{13}C NMR, ESI-MS and IR spectra. The purity of each compound was ascertained by means of elemental analysis. The molecular structure of **10** was additionally confirmed by using APCI–HRMS, (Atmospheric Pressure Chemical Ionization–High Resolution Mass Spectrometry), detailed assignments of NMR signals and ROESY cross-peaks (see Figs. S1, S2 and S3, respectively in Supplementary data).

2.2. Crystallography

The structures of compounds **2** and **9** with the atomic numbering scheme are shown in Figs 2 and 3, respectively. Crystal data, data collection and structural refinement details are given in Table S1 (Supplementary data).

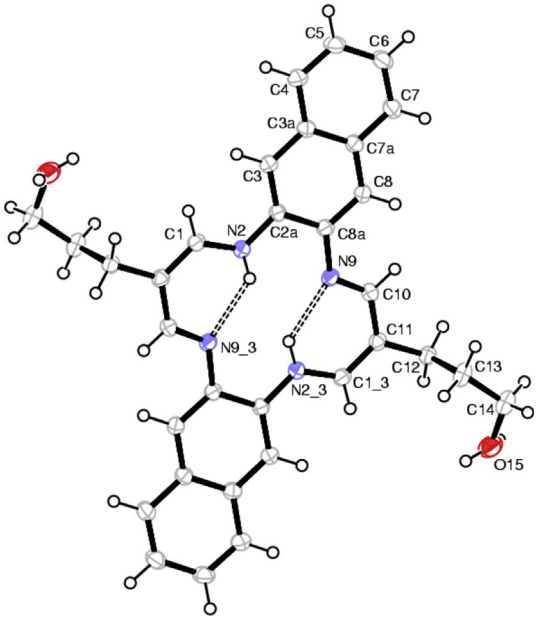

Fig. 2. The view of molecule **2** with the atom numbering scheme at 120 K. Atomic displacement ellipsoids are drawn at 50% probability level. Hydrogen atoms are drawn with an arbitrary radius. The molecule is centrosymmetric with the centre at (0 ½ 0). The valence angles C8a-N9-C10=120.2(1) and C1–N2–C2a=124.6(1) clearly indicate the localization of H atom at N2. Hydrogen atom at O15 (hydroxyl terminal group) is disordered between two positions with site occupancy 0.5. Index _3 denotes symmetry code ($-x$, $-y+1$, $-z$). Intramolecular hydrogen bonds are marked by dotted line.

Compound **2** ($C_{32}H_{32}N_4O_2$) crystallizes in the monoclinic space group $P2_1/c$ (Z=2) with half of the molecule in the asymmetric part of the unit cell as the molecule is centrosymmetric. The 14-membered ring of **2** is nearly planar with the distortion from planarity of 0.0528 Å (r.m.s deviation of the fitted atoms) and with the angle between pentadiimine moiety and the naphthalene system of 11.17(8)°. The propyl moiety best plane of 3-hydroxypropyl substituent in *meso* position is inclined 83.05(10)° against the tetraaza [14]annulene ring.

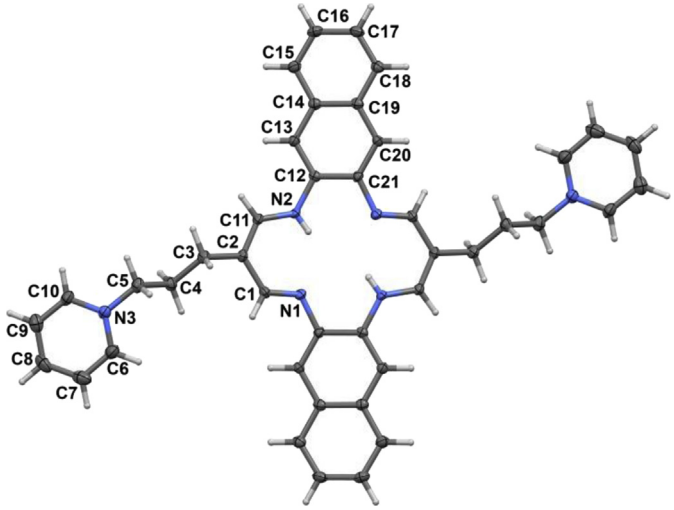

Fig. 3. The structure of macrocyclic cation of compound **9** at 100 K, showing 50% probability displacement ellipsoids with the atom numbering scheme. Hydrogen atoms are drawn with an arbitrary radius.

The character of bond lengths within the 14-membered ring could be considered in two fragments: the first containing the alternate bonds in sequence single-double-single: N9–C8a=1.410(2), N9-C10=1.318(2) and C10-C11=1.421(2) Å and the second, C2a-N2=1.399(2), N2-C1=1.340(2), C1-C11$^{(-x,\ -y+1,\ -z)}$=1.380(2) Å, indicating partial electron delocalisation (Table S2 in Supplementary data). The difference is caused by the engagement of the N9 lone pair in the intramolecular hydrogen bond N2–H2…N9$^{(-x,\ -y+1,\ -z)}$ (Table 3), whereas the N2 lone pair is incorporated into coupled system. The values of the appropriate valence angles at nitrogen atoms N2 and N9: C1–N2–C2a=124.6(1) and C8a–N9–C10=120.3(1)°, confirmed H-atom localization at N2.

Packing of molecule **2** shown in Fig. 4 in the structure is governed by intermolecular O–H···O, and weak C–H···π and π···π interactions[12] with the geometry given in Table 1.

The shortest lattice period, a=4.8827(1) Å, is defined by hydrogen bond system of O–H···O type between hydroxyl groups aligned along [100]. The hydrogen atoms are disordered and were refined with the site occupancy 0.5. The disorder is static as diffraction experiment was performed at 120 K (see Fig. 5).

Table 1
Hydrogen bond geometry and selected weak interactions (Å, °)

	D–H	H…A	D…A	∠DHA
2				
N2-H2…N9$^{(-x,\ -y+1,\ -z)}$	0.87 (1)	2.10 (1)	2.756 (2)	132 (2)
O15-H15a…O15$^{(-x+2,\ -y+1,\ -z+1)}$	0.84 (1)	2.00 (2)	2.802 (3)	157 (4)
O15-H15b…O15$^{(-x+1,\ -y+1,\ -z+1)}$	0.85 (1)	2.01 (1)	2.859 (3)	174 (5)
C6-H6…Cg3$^{(x+1/2,\ -y+3/2,\ z-1/2)}$	0.95	3.28	4.126	149
C12-H12a…Cg3$^{(x+1,\ y,\ z)}$	0.99	2.84	3.613	135
Cg3…Cg3$^{(-x+1,\ -y+1,\ -z)}$	—	—	3.762 (2)	—
π…Cg3$^{(-x+1,\ -y+1,\ -z)}$	—	—	3.313 (2)	—
Ring gravity centre: Cg3 for N9C10C11C1$^{(-x,\ -y+1,\ -z)}$N2$^{(-x,\ -y+1,\ -z)}$, π system of N9C10C11C1$^{(-x,\ -y+1,\ -z)}$N2$^{(-x,\ -y+1,\ -z)}$ moiety				
9				
N2-H2…N9$^{(-x+1,\ -y,\ -z+2)}$	0.73 (5)	2.16 (4)	2.733 (4)	137 (4)
O1-H22…Br1	0.84	2.53	2.718 (4)	161
C5-H5B…Br1	0.99	2.80	3.754 (4)	162
C10-H10…Cg1$^{(x+1,\ -y+2,\ z+½)}$	0.95	2.49	3.324 (4)	146
Cg1…Cg2$^{(x+1,\ y,\ z+1)}$	—	—	3.617 (2)	—
π…Cg2$^{(x+1,\ y,\ z+1)}$	—	—	3.513 (2)	—
Ring gravity centres: Cg1 for C12C13C14C19C20C21 and Cg2 for N3C6C7C8C9C10; π system of C12-C21 ring				

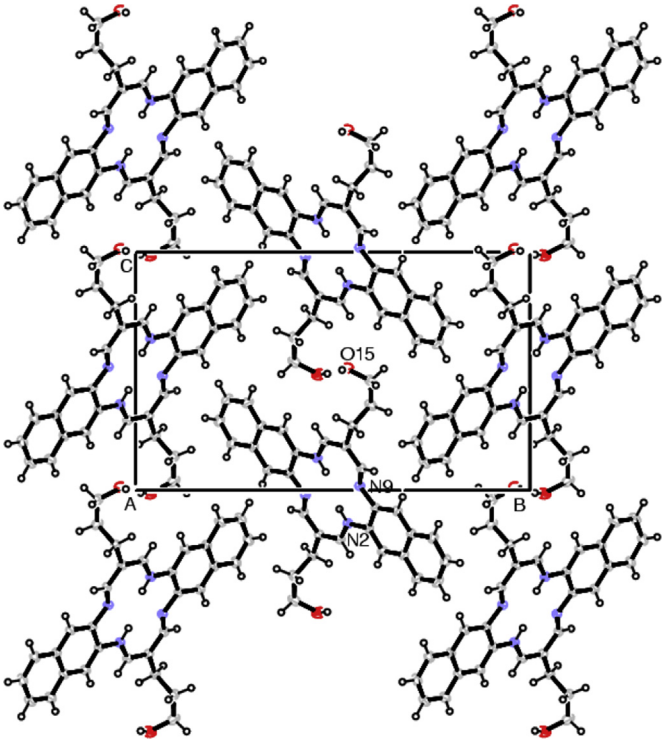

Fig. 4. Packing of the molecules **2** viewed along a-axis.

Only the π system of pentadiimine moiety acts as acceptor of two weak C–H···π interactions (Table 1). Moreover there is a π-stacking between the pentadiimine moieties related by (−*x*+1,−*y*+1,−*z*) with the distance between the neighbouring gravity centres of 3.762(2) Å marked in Fig. 6. The strength of this interaction is illustrated by a very short, 3.313(2) Å, interplanar distance.

Compound **9** crystallizes in the monoclinic $P2_1/c$ space group with one half of the macrocyclic cation, one bromide anion and one methanol solvent molecule in the asymmetric part of the unit cell. The central 14-membered ring of the macrocycle moiety is situated across a centre of inversion (Fig. 3). The macrocycle adopts a step-like conformation, with the r.m.s deviation of 14 fitted atoms of the tetraaza ring being 0.165 Å (Fig. 7). This deviation from planarity

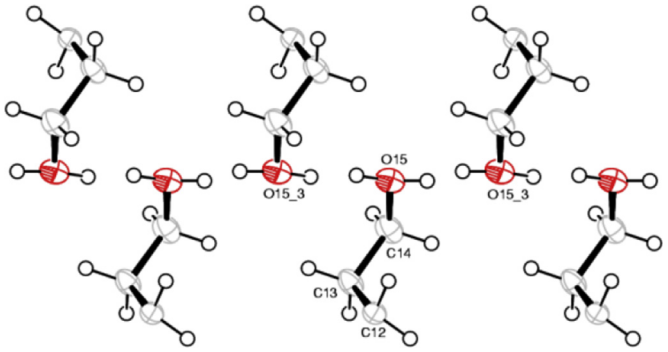

Fig. 5. 3-hydroxypropyl group alignment along *a* -axis (other atoms are removed for clarity). On the left side of O15 is the hydroxyl group transformed by (−*x*−1,−*y*,−*z*) and on the right that one at (−*x*+1,−*y*,−*z*). Note the disordered hydrogen atoms (static disorder) with site occupancy 0.5 each. The geometry of relatively strong hydrogen bonds is given in Table 1.

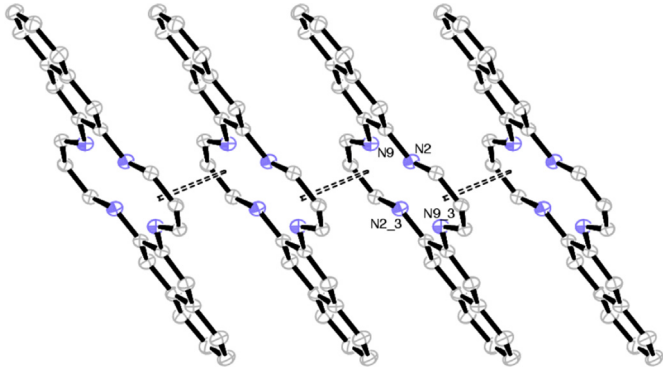

Fig. 6. Stacking observed between pentadiimine moieties of **2**. The distance 3.762(2) Å between the gravity centres of neighbouring pentadiimine system related by (−*x*+1,−*y*+1,−*z*) is marked by dashed lines. Two *meso* substituents and all hydrogen atoms are omitted for clarity. Index _3 denotes symmetry code (−*x*, −*y*+1, −*z*).

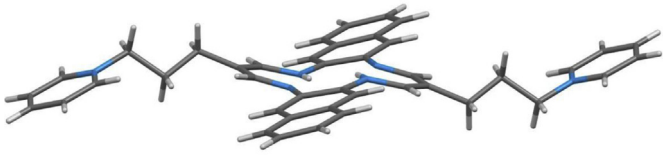

Fig. 7. A step-like conformation of the tetraaza[14]annulene macrocycle in **9**.

seems to be caused by relatively strong C–H···π interactions between the adjacent molecules. The intermolecular C10-H10···C(12-13-14-19-20-21)$^{1+x,\ 3/2-y,\ ½+z}$ ring contact with C10···centroid distance is 3.324(4) Å.

The supramolecular structure is completed by C–H···Br, O–H···Br, C–H···π and π···π stacking interactions, as shown in Fig. 8. The bromide anion is linked to the methanol solvent molecule by O–H···Br hydrogen bond. Packing of the molecules **9** is shown in Figs. S4a and S4b (Supplementary data).

The pyridine ring is involved in a face-to-face π···π stacking interaction with the naphthalene ring system π···Cg2$^{1+x,\ y,\ 1+z}$ distance being 3.513(2) Å. The dihedral angle between the naphthalene and pyridine planes is 7.0(2)°. The aliphatic chain connecting tetraaza and pyridine rings adopts a distinct planar, extended conformation with torsion angles of −171.5(3) and 176.9(3)° for C2–C3–C4–C5 and C3–C4–C5–N3, respectively. These geometric parameters are similar to those observed in previously reported structures of the dibenzotetraaza[14]annulene

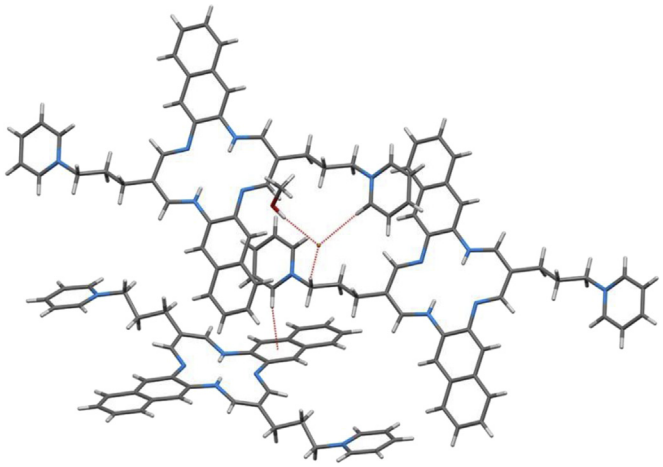

Fig. 8. Three intermolecular C–H···Br, O–H···Br and C–H···π contacts in **9**, shown as dashed lines.

derivatives equipped with 3-(*N*-pyridinium-1-yl)propyl and 3-(4,4-bipyridinium-1-yl)propyl substituents.[4a]

The localization of N2-bonded hydrogen atom found in the difference Fourier map analysis has been confirmed by the valence angles at nitrogen atoms of 118.4(3) and 124.5(3)°, for N1 and N2, respectively.

Summing up, in the crystal structures of **2** and **9** the pseudo-hexagonal packing of the molecules is governed by specific C–H···π and π···π interactions. In the case of **2** the pentadiimine moiety plays a major role in the intermolecular interaction (stacking mode) whereas in **9** the weak interactions appear between one ring of naphthalene system and pyridinium ring and are responsible for 3-dimensional packing of the molecules. It should be noted that in the structure of **2** strong intermolecular hydrogen bonds of O–H···O with the static disorder of H-atom positions force very short period of *a*.

2.3. UV–vis spectroscopy and quantum chemical calculations

UV–vis spectra for all compounds were simulated based on calculated excitation energies as superpositions of Gaussian peaks with heights corresponding to oscillator strengths placed at transition energies; standard deviations of individual curves were set to 1300 cm^{-1}. The latter value was chosen to obtain the width and the shape of absorption bands similar to experimental spectra (upper panel of Fig. 9. Simulated absorption spectra are displayed in the lower panel of Fig. 9. As readily seen, spectra obtained from TDDFT computations agree with experimental data. Absorption maxima for all compounds **6**–**8** are located at similar wavelengths (382–383 nm in the experiment, 396–398 nm calculated). For **9** the main maximum is shifted to longer wavelengths and another weaker transition is noticeable slightly below 500 nm. Although there is a difference between theory and experiment in the position of the main band for **6**–**8** and the shift of the main maximum to longer wavelengths computed for **9** is smaller than in experiment, calculated data capture well the major features of measured absorption spectra providing satisfactory reproduction of the experiment.

The difference between **9** and compounds **6**–**8** was analyzed in more details using **8** as a sample case. In Fig. 9, excitation energies and their relative oscillator strengths are marked for **8** and **9** with vertical lines. There are two or three intensity-carrying transitions in the region 380–500 nm (and a number of transitions with negligible absorption intensity). In compound **8** the long-wavelength transition is weaker than in **9** and it is located at

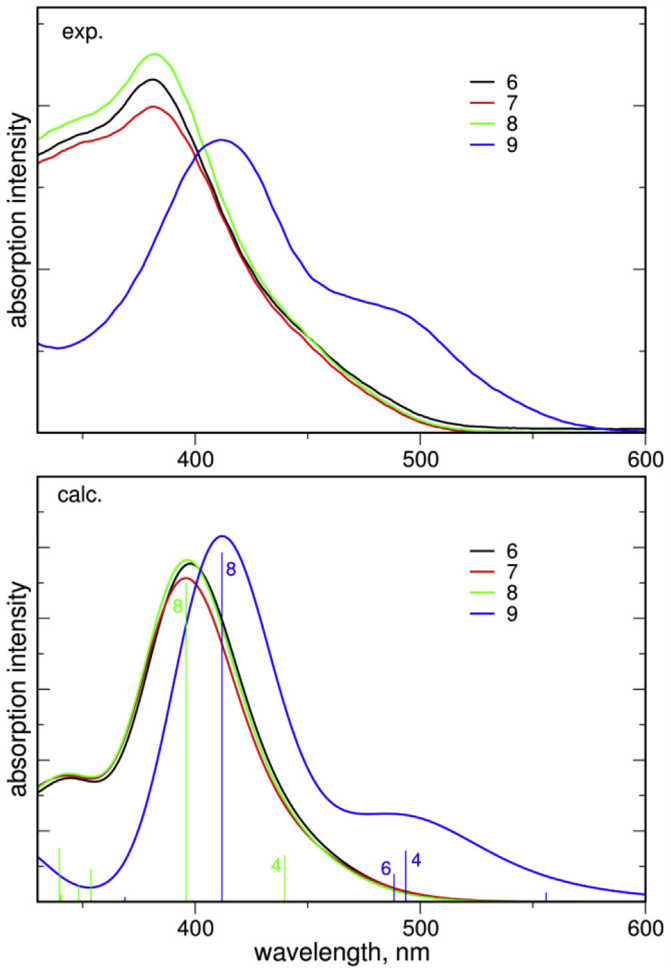

Fig. 9. Experimental and calculated absorption spectra for **6**–**9**. Vertical lines in the lower panel mark the energies and relative oscillator strengths of individual transitions for **8** and **9**.

440 nm, not very far from the main transition at 396 nm and therefore not discernible from the shoulder of the main absorption band. In **9**, the intensity of this transition is larger and its position changes to 493 nm, simultaneously another transition with non-zero intensity appears at 488 nm, therefore the long-wavelength part of the spectrum acquires intensity and becomes observable in the experiment.

In Fig. 10, dominant Natural Transition Orbitals[13] (i.e., orbitals transformed to obtain maximum correspondence between 'initial' and 'final' orbital of the transition) pairs are displayed for the two bright transitions of both molecules. In all cases orbitals involved in the transition have a nodal plane in the plane of the macrocycle, thus exhibit π symmetry; accordingly observed transitions are of $\pi \rightarrow \pi^*$ type. Electron density of all orbitals shown in Fig. 10 is located mainly on the macrocycle ring and naphthalene moieties. In the final orbital of the main transition of both molecules it concentrates even more on the tetraazaannulene core. The difference between **9** and **8** is that for compound **8** (as well as for **6** and **7** not shown in the plot) there is small electron density of the initial orbital (more noticeable for the long-wavelength transition) located on the oxygen atom of the side chain of the molecule, whereas in molecule **9** electron density on the aliphatic side chain is negligible. Inspection of frontier orbital energies for **8** and **9** shows that in both molecules LUMO have almost the same energies but the energy of the HOMO is lower in compound **8**, increasing the HOMO-LUMO splitting. Although this value does not correspond directly to

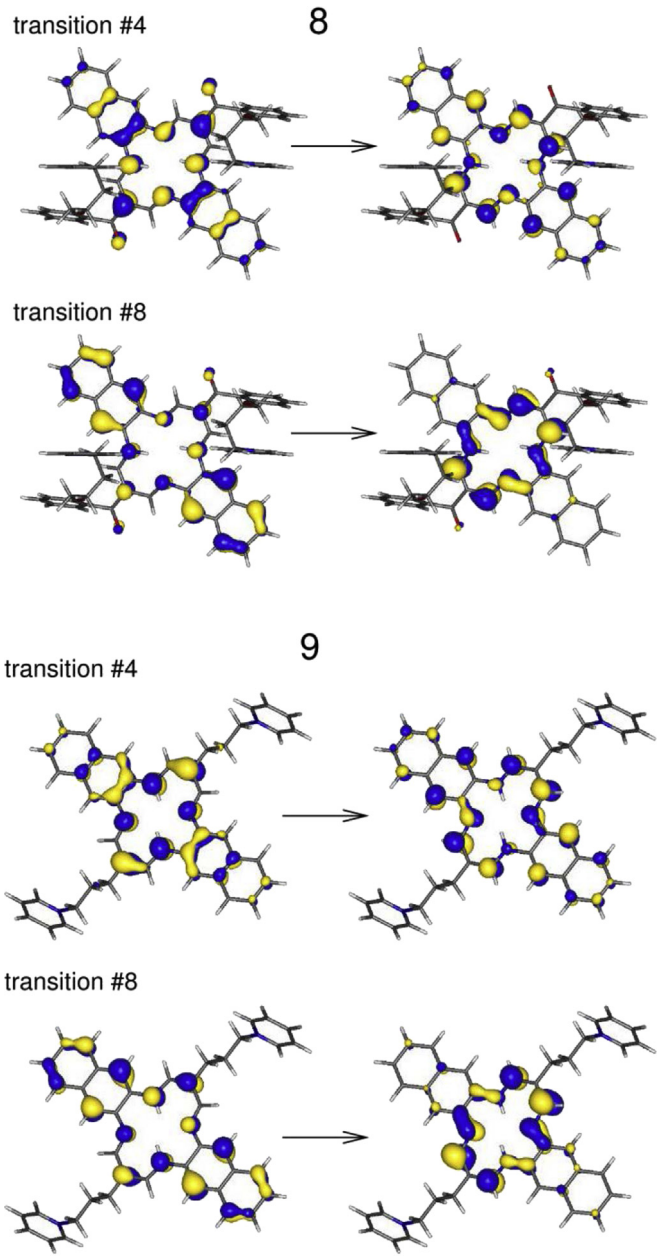

Fig. 10. Dominant Natural Transition Orbital pairs obtained for electronic transitions in 8 and 9. Transitions numbered according to Fig. 9.

measured transition energy, both values are correlated and the HOMO-LUMO gap may serve as a rough estimate for excitation energy. Therefore we may conclude that larger delocalization of occupied orbitals in **8** (with electron density on the benzoyl oxygen atom) lowers their energies thus increasing the energy of the optical transition and decreasing the wavelength of the absorption band.

2.4. Interactions of 8 with polynucleotides in aqueous medium

2.4.1. Spectrophotometric properties of 8 in aqueous medium.- Compound **8** is moderately soluble in aqueous solutions (up to $c=1\times10^{-3}$ mol dm^{-3}, buffered aqueous solutions were stable for longer periods. The absorbencies of **8** in buffered aqueous solution (pH 7.0, sodium cacodylate/HCl buffer, I=0.05 mol dm^{-3}, Fig. S5, Table S3 in Supplementary data) are proportional to concentration up to $c=2\times10^{-5}$ mol dm^{-3}, changes of the UV–vis spectra on the temperature increase up to 95 °C were negligible and reproducibility of UV–vis spectra upon cooling back to 25 °C was excellent.

At variance to previously studied DBTAA derivatives,[4c,d] the aqueous solution of DNTAA derivative **8** exhibited fluorescence (Fig. 12), which is attributed to the naphthalene chromophore.

2.4.2. Study on interactions with double stranded (ds)-DNA.- Addition of calf thymus DNA (ct-DNA), poly(dA-dT)$_2$ and poly(dG-dC)$_2$ resulted in strong bathochromic and hypochromic effects in the UV–vis spectrum of **8** (Fig. 13, Table 2, Figs. S6–8, Supplementary data). In addition, we performed fluorescence titrations and processed the titration data by Scatchard equation[14] to obtain binding constants log*Ks* and Scatchard ratios, n$_{[\text{bound }\mathbf{8}]/[\text{DNA}]}$ (Table 2). Comparison of binding data revealed somewhat lower DNA affinity of **8** in comparison to its close DBTAA analogue **DBTAA-8** (see Fig. 11). Moreover, rather high values of Scatchard ratio *n* suggest aggregation at high excess of compound over DNA. To assess in more detail the structural aspects of DNA binding and possible mixed binding modes at various ratios *r*=[**8**]/

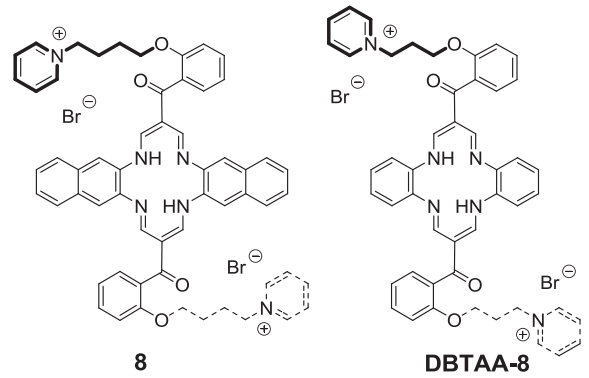

Fig. 11. Structures of a new DNTAA derivative **8** and of its *o*-phenylene analogue **DBTAA-8**, studied previously.[4c,d]

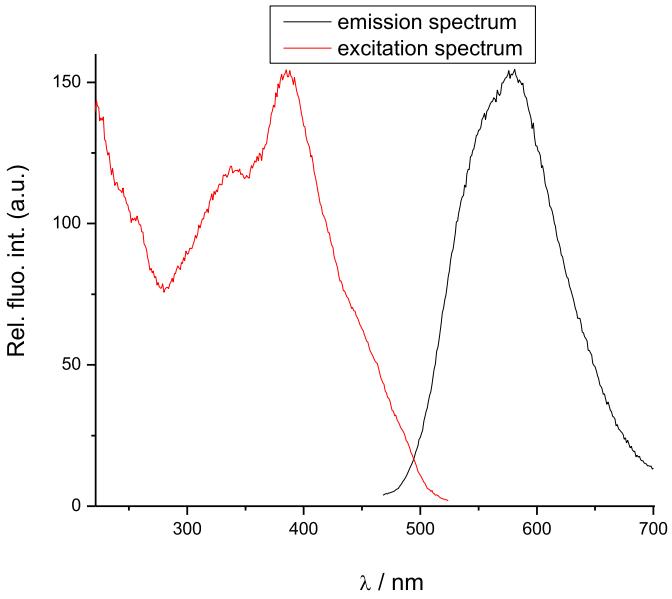

Fig. 12. Excitation and emission spectra of **8**, c(**8**)=5×10^{-6} mol dm^{-3}, at pH=7, buffer sodium cacodylate, I=0.05 mol dm^{-3}. Excitation spectrum agrees well with the UV–vis spectrum. Excitation spectrum was recorded by monitoring emission at λ_{max}=579 nm in the range from 220 to 525 nm and emission spectrum was recorded by monitoring emission from 470 to 700 nm with excitation at λ_{max}=382 nm.

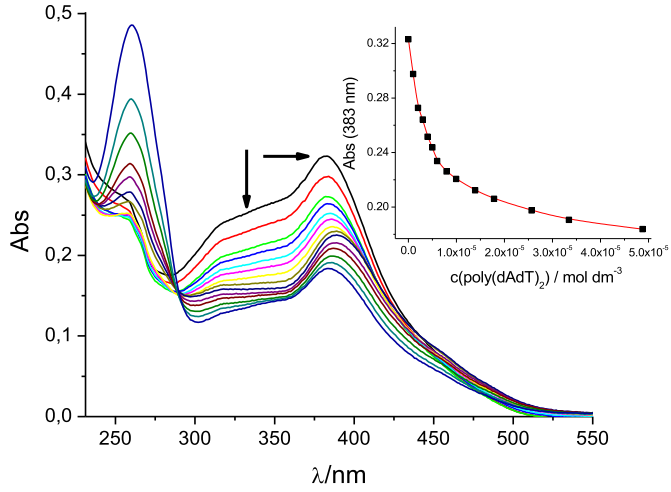

Fig. 13. Changes in the UV–vis spectrum of **8** (c=7.0×10^{-6} mol dm^{-3}) upon titration with poly(dA-dT)$_2$ (c=1×10^{-6}–4.9×10^{-5} mol dm^{-3}); b) Dependence of **8** absorbance at λ_{max}=383 nm on c(poly(dA-dT)$_2$), at pH 7.0, sodium cacodylate buffer, I=0.05 mol dm^{-3}.

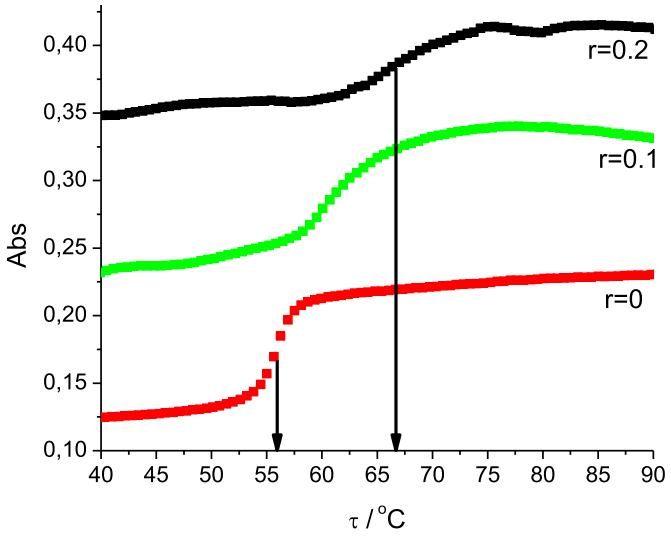

Fig. 14. Thermal melting curve of poly(dA-dT)$_2$ upon addition of r$_{[8]/[polynucleotide]}$=0; 0.1; 0.2 at pH 7.0 (buffer sodium cacodylate, I=0.05 mol dm^{-3}) b) first derivation of absorbance on temperature.

[polynucleotide], we performed CD experiments (Fig. 15 and 2.4.4. CD experiments, Figure S10 in Supplementary data).

Table 2
Binding constants (log*Ks*)[a] and ratios n[b] ([bound compound]/[polynucleotide]) calculated from the UV–vis titrations of **8** with ds-polynucleotides at pH 7.0 (buffer sodium cacodylate, I=0.05 mol dm^{-3})

	poly(dAdT)$_2$			ctDNA			poly(dGdC)$_2$		
	H/%[c]	log*Ks*	n	H/%[c]	log*Ks*	n	H/%[c]	log*Ks*	n
8	41.8	5.98	0.87	22.4	7.41	0.61	31.9	6.61	1.08
[e]**DBTAA-8**	[d]26	[d]7.21	[d]0.24	25	8.92	0.37	—	—	—

[a] Titration data were processed according to the Scatchard equation.
[b] Accuracy of n±10–30%, consequently log*Ks* values vary in the same order of magnitude.
[c] H=(Abs(**8**)–Abs(complex))/Abs(**8**))×100.
[d] Poly dA–poly dT.
[e] Published results.[4c,d]

Addition of ds-DNA induces threefold increase of **8** fluorescence, irrespective of DNA-basepair composition and secondary structure. Thus, DNTAA derivatives offer intriguing new applications (in respect to DBTAA analogues) as fluorescence DNA/RNA dyes and will be studied in more detail within future research.

2.4.3. Thermal melting experiments. Thermal denaturation data (Fig. 14, Table 3, Fig. S9, Supplementary data) revealed that compound **8** strongly stabilised AT-DNA and much more weakly stabilised ctDNA (42% of GC-basepairs), pointing out some basepair dependence. Replacement of benzene in **DBTAA-8** with naphthalene in **8** decreased thermal stabilisation effect.

Table 3
The[a]ΔT_m values (°C) of studied ds-polynucleotides upon addition of ratio [b]***r*** of **8** and [c]DBTAA-8 at pH 7.0 (sodium cacodylate buffer, I=0.05 mol dm^{-3})

[a]ΔT_m/°C	[b]r	poly(dA-dT)$_2$	ctDNA
8	0.2	8.7	1.3
[c]**DBTAA-8**	0.2	[d]28.1	10.7

[a] Error in ΔT_m: ±0.5 °C.
[b] r=[compound]/[polynucleotide].
[c] Published results.[4c,d]
[d] Poly dA–poly dT, r=0.3.

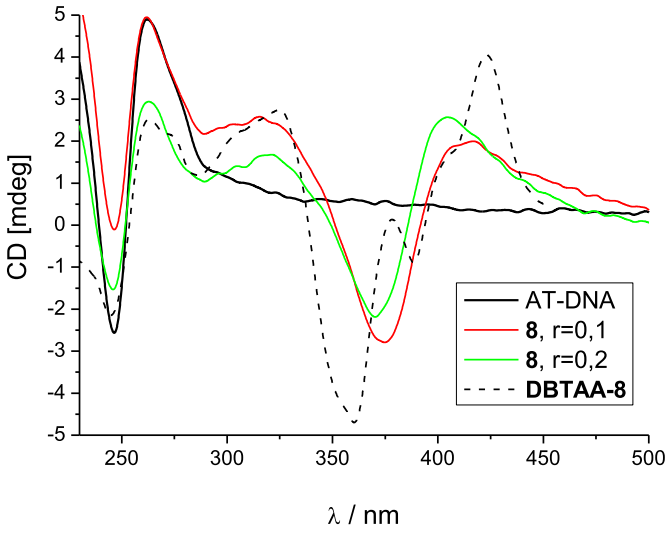

Fig. 15. CD titration of poly (dAdT)$_2$ (full black line; c=3.0×10^{-5} mol dm^{-3}), with **8** (red, green line) and **DBTAA-8** (dash black) at several molar ratios ***r***=[compound]/[polynucleotide] (pH 7.0, buffer sodium cacodylate, I=0.05 mol dm^{-3}).

2.4.4. Circular dichroism (CD) experiments. The CD spectra of the ligand-polynucleotide complexes can provide information on two levels.[15] First, the conformation of polynucleotide itself can be probed through the CD of the intrinsic polynucleotide absorption near 260 nm. Second, achiral small molecules acquire an induced CD (ICD) signal when they form complexes with a polynucleotide from, which a mutual orientation of small molecule and polynucleotide chiral axis could be derived, consequently giving useful information about modes of interaction.[16] It should be noted that studied compound **8** is achiral and therefore does not possess an intrinsic CD spectrum.

Addition of **8** resulted in a decrease of CD spectra in the 245–300 nm range, attributed to the CD bands of DNA polynucleotides (Fig. S10, Supplementary data), usually associated with partial disruption of polynucleotide helical chirality caused by the binding of a small molecule.

Upon mixing **8** with any of the studied ds-DNA, ICD signals appeared in the 300–550 nm range, agreeing well with the UV–vis spectrum (Fig. 13). For AT-DNA the shape of ICD bands depended strongly on the ratio *r*: for excess of DNA over **8** ($r<0.3$) ICD bands pattern (Fig. 15, Fig. S10a and S10a1 in Supplementary data) resembled closely to the ICD of DBTAA analogue **DBTAA-8**[4d] and therefore intercalative binding mode can be presumed. At an excess of **8** over the concentration of intercalative binding sites (ratios $r>0.3$, Fig. S10, Supplementary data) the ICD pattern significantly changed due to the aggregation of small molecules along DNA—behaviour characteristic for **8** but not for **DBTAA-8**. At variance to AT-DNA, complexes of **8** with the GC-DNA and mixed sequence ct-DNA (42% GC-basepairs) didn't show dependence of ICD bands on ratio *r*, only one ICD pattern was observed (Fig. S10, Supplementary data) with isoelliptic points suggesting one dominant type of binding. Again, the similarity of ICD pattern with **DBTAA-8** supported intercalative binding mode. The reason why ICD bands of compound **8** at $r>0.3$ show aggregation along AT-DNA but not along GC-rich DNA could be correlated to the differences in DNA secondary structure, whereby the size of the AT-DNA minor groove (6.4 A width) is much more convenient for aggregation of small molecules than GC-DNA (severely hindered by protruding amino groups of guanine).[17]

3. Conclusions

Single crystal X-ray measurements of **4** and **8**, reported previously, revealed molecules consisting of a large planar core bearing two *meso*-attached side groups folded above and below the plane.[8] Compounds **2** and **9** have a more relaxed arrangement of the side chains allowing unhindered access to the naphthalene and pentadiiminate moieties, and therefore seem to be well suited for intercalation in DNA.

Electronic structures of the new products and differences between their absorption spectra were discussed based on quantum-chemical calculations employing DFT methodology.

Changing from previously studied DBTAA to naphthalene analogues DNTAA introduced several intriguing properties for bio-oriented studies. The naphthalene in the DNTAA moiety introduced fluorescence in aqueous medium, whereby DNTAA (**8**) binding to ds-DNA increased emission by threefold. Thus, DNTAA derivatives offer intriguing new applications (in respect to DBTAA analogues) as fluorescence DNA/RNA dyes and will be studied in more detail within future research. Novel DNTAA derivatives bind ds-DNA similarly to previously studied DBTAA, by intercalation. Surprisingly, the increased aromatic surface of naphthalene (DNTAA) in comparison to benzene (DBTAA) didn't yield higher affinity or stronger thermal stabilisation effects; actually a minor affinity decrease was observed. It seems that the aromatic surface of basepairs controls the efficiency of aromatic stacking interactions and consequently affinity, whereas larger naphthalene subunits are actually at a disadvantage due to the steric hindrance to efficient intercalation between the DNA basepairs. At an excess of dye over DNA binding sites DNTAA derivative tends to aggregation along all studied ds-DNA as shown in fluorescence and UV–vis titrations.

4. Experimental section

4.1. General

Compounds **1**, **4** and **8** were prepared by the procedure described earlier.[8] 2,3-Diaminonaphthalene, 3-formylchromone 1,3-dibromopropane, 1,4-dibromobutane and tetrabromomethane were purchased from commercial sources (Sigma–Aldrich, AlfaAesar) and were used as received. Solvents were dried using standard methods and were freshly distilled before use.

Elemental analyses were performed on an Elementar Vario MICRO cube analyser. 1H and 13C NMR spectroscopy was performed using a Bruker AVANCE II 300 and Bruker AVANCE III 600 spectrometers. Chemical shifts (δ) are expressed in parts per million and J values in hertz. Signal multiplicities are denoted as s (singlet), d (doublet), t (triplet), q (quartet), and m (multiplet). ESI mass spectra were taken on a Bruker Daltonics Esquire 3000 spectrometer. HRMS spectrum were taken on a Bruker MicroTOF-QII, UV–vis spectra were measured using a Hitachi U–3900H spectrophotometer. The IR-ATR spectra were recorded with a Thermo Fisher Scientific Nicolet IR200. Melting points were measured using a Boethius apparatus and were not corrected.

4.2. Syntheses

*4.2.1. 9,20-Bis(3-hydroxypropyl)-7,18-dihydrodinaphtho[b,i][1,4,8,11]tetraazacyclotetradecine **2**.* A reaction mixture consisting of 2,3-diaminonaphthalene (0.75 g, 4.74 mmol), 3,4-dihydro-2*H*-pyran-5-carbaldehyde (0.53 g, 4.74 mmol) and n-butanol (15 mL) was refluxed under argon for 12 h. A red, fairly insoluble precipitate was filtered off and washed thoroughly with ethanol and diethyl ether. Red microcrystals, yield 0.25 g (42%), mp 312–316 °C (decomposition). Analytical sample was recrystallized from DMF. Crystals suitable for X-ray measurements were grown from DMF. **^{1}H NMR (300 MHz, DMSO-d_6, δ ppm):** 1.76 (m, 4H, C$\underline{H}_2$CH$_2$O), 2.46 (m, 4H, CH$_2$), 3.54 (m, 4H, CH$_2$O), 4.51 (t, *J*=5.0 Hz, 2H, OH), 7.31 (m, 4H, Ar–H), 7.72 (m, 4H, Ar–H), 7.85 (s, 4H, H^{1,6,12,17}), 8.26 (d, *J*=6.0 Hz, 4H,=CHN), 12.72 (t, *J*=6.0 Hz, 2H, NH); **^{13}C NMR (75 MHz, DMSO-d_6, δ ppm):** 28.78 (C$\underline{H}_2$CH$_2$O), 35.34 (CH$_2$), 59.87 (CH$_2$O), 108.86, 109.88, 124.82, 126.89, 131.05, 136.91 (C$_{aromat.}$N), 148.47 (=CHN); **IR (ATR) ν_{max}(cm^{-1}):** {3372, 3311} (OH), {3194, 3176} (NH), 3053 (Ar–H), {2941, 2928, 2872} (CH$_2$), {1640, 1620, 1596, 1547} (C=N, Ar), 1297, 1272 (C–O); **ESI-MS**: (*m*/*z*) 505.4 (M+H$^+$); **Anal. Calcd for $C_{32}H_{32}N_4O_2$**: C, 76.16; H, 6.39; N, 11.10. Found: C, 75.80; H, 6.45; N, 11.15%.

*4.2.2. 9,20-Bis[2-(3-bromopropoxy)benzoyl]-7,18-dihydrodinaphtho[b,i][1,4,8,11]tetraazacyclotetradecine **3**.* A reaction mixture consisting of **1** (0.3 g, 0.48 mmol), 1,3-dibromopropane (0.5 mL, 4.8 mmol), potassium carbonate (0.5 g) and DMF (70 mL) was stirred at room temperature for 48 h. It was then transferred to a separatory funnel and partitioned between dichloromethane (40 mL) and water (50 mL). The organic phase was separated, washed with water (4×50 mL), dried over anhydrous MgSO$_4$, then concentrated to a small volume and diluted with n-hexane (20 mL). A yellow precipitate was filtered off, dried and then chromatographed on a column of silica gel using dichloromethane–acetone (40:1) as eluent. The main yellow fraction was collected, concentrated to a small volume and left to crystallise. Orange crystals were collected and dried, yield 0.18 g (38%), mp 272 °C. **^{1}H NMR (600 MHz, CDCl$_3$, δ ppm):** 2.21 (m, 4H, CH$_2$), 3.44 (t, *J*=6.3 Hz, 4H, CH$_2$Br), 4.18 (t, *J*=5.7 Hz, 4H, CH$_2$O), 7.09 (d, *J*=8.4 Hz, 2H, H$^{26,26'}$), 7.14 (ddd, *J*=7.4 Hz, *J*=7.4 Hz, *J*=0.9 Hz, 2H, H$^{28,28'}$), 7.39 (m, 4H, H^{3,4,14,15}), 7.46 (dd, *J*=7.4 Hz, *J*=1.7 Hz, 2H, H$^{29,29'}$), 7.50 (ddd, *J*=8.4 Hz, *J*=7.4 Hz, *J*=1.8 Hz, 2H, H$^{27,27'}$), 7.61 (s, 4H, H^{1,6,12,17}), 7.72 (m, 4H, H^{2,5,13,15}), 8.86 (b. s 4H, N=C–H), 13.98 (br s, 2H, NH); **^{13}C NMR (151 MHz, CDCl$_3$, δ ppm):** 30.09 (CH$_2$), 32.26 (CH$_2$Br), 66.23 (CH$_2$O), 111.23, 112.87, 113.11, 121.63, 126.33, 127.68, 129.61, 129.71, 131.63, 132.12, 136.90, 153.63 (C^{25}O), 155.75 (=CHN), 193.16 (C=O); **IR (ATR) ν_{max}(cm^{-1}):** 3053 (Ar–H), 2959 (CH$_2$), {1652, 1608, 1594, 1563} (C=O, C=N, Ar), {1290, 1262} (C–O); **ESI-MS**: (*m*/*z*) 869.2 (M+H$^+$); **Anal. Calcd for $C_{46}H_{38}Br_2N_4O_4$**:C, 63.46; H, 4.40; N, 6.44. Found: C, 63.73; H, 4.50; N, 6.40%.

*4.2.3. 9,20-Bis[3-bromopropyl]-7,18-dihydrodinaphtho[b,i][1,4,8,11]tetraazacyclotetradecine **5**.* Compound **2** (0.25 g, 0.5 mmol) was

dissolved in DMF (50 mL) with gentle heating. After the solution was cooled to room temperature, tetrabromomethane (0.66 g, 2 mmol) and triphenylphosphine (0.53 g, 2 mmol) were added, and the mixture was stirred under argon at room temperature for 24 h. A small amount of the final product was isolated at this stage as a fairly insoluble red precipitate. It was filtered off and washed with hot methanol. The filtrate was transferred to a separatory funnel and partitioned between dichloromethane (150 mL) and water (100 mL). The organic layer was separated, washed with water (3×100 mL) then dried over anhydrous $MgSO_4$ and chromatographed on a column with silica gel using CH_2Cl_2 as eluent. The main red fraction was collected, concentrated to a small volume and left overnight in a refrigerator to crystallise. Red precipitate was collected and dried, yield 0.2 g (63%), mp 261–262 °C. **^{1}H NMR (300 MHz, $CDCl_3$, δ ppm):** 2.17 (m, 4H, C$H_2$$CH_2$Br), 2.60 (t, *J*=7.1 Hz, 4H, CH_2), 3.56 (t, *J*=6.4 Hz, 4H, CH_2Br), 7.32 (m, 4H, Ar–H), 7.51 (s, 4H, $H^{1,6,12,17}$), 7.68 (m, 4H, Ar–H), 8.05 (s, Hz, 4H, N=C–H); **IR (ATR) ν_{max}(cm^{-1}):** {3194, 3176} (NH), 3046 (Ar–H), {2963, 2887 } (CH_2), {1641, 1619, 1594, 1547} (C=N, Ar); **ESI-MS**: (*m*/*z*) 629.4 ($M+H^+$); **Anal. Calcd for $C_{32}H_{30}Br_2N_4$**: C, 60.97; H, 4.80; N. 8.89. Found: C, 60.58; H, 4.79; N, 8.70%.

4.2.4. 9,20-Bis{2-[4-(N,N,N-trimethyloammonium)butoxy]benzoyl}-7,18-dihydrodinaphtho[b,i][1,4,8,11]tetraazacyclotetradecine dibromide trihydrate ***6***. To a suspension of compound **4**[8] (0.13 g, 0.14 mmol) in DMF (60 mL), cooled to −10 °C, trimethylamine (2 mL, 21 mmol) was added and the mixture was stirred at 45 °C under argon for 36 h. The solvent was removed using a rotary evaporator, methanol (2 mL) was added to the oily residue and a small quantity of *tert*-butyl methyl ether (0.5 mL). The mixture was left overnight in a refrigerator. Yellow precipitate was filtered off, dried and recrystallized from the mixture methanol–dichloromethane (10:1) layered with *tert*-butyl methyl ether. Pale-yellow microcrystalline product was collected after 3 days, yield 0.76 g (51%), mp 230–233 °C. **^{1}H NMR (300 MHz, DMSO-d_6, δ ppm):** 1.64 (m, 8H, $CH_2^{b,c}$), 2.86 (s, 18H, CH_3), 3.20 (m, 4H, CH_2N^+), 4.17 (t, *J*=5.6 Hz, 4H, CH_2O), 7.16 (dd, *J*=7.4, 7.4 Hz, 2H, $H^{28,28'}$), 7.29 (d, *J*=8.4 Hz, 2H, $H^{26,26'}$), 7.44 (m, 6H, $H^{3,4,29,29',14,15}$), 7.59 (m, 2H, $H^{27,27'}$), 7.82 (s, 4H, $H^{1,6,12,17}$), 7.86 (m, 4H, $H^{2,5,13,16}$), 8.85 (d, *J*=6.4 Hz, 4H, N=C–H), 13.82 (t, *J*=6.5 Hz, 2H, NH); **^{13}C NMR (75 MHz, DMSO-d_6, δ ppm):** 18.96 (CH_2), 25.50 (CH_2), 51.78 (CH_3), 64.77 (CH_2O), 67.34 (CH_2N^+), 110.43, 112.78, 113.03, 121.02, 126.28, 127.56, 128.69, 129.43, 131.53, 131.81, 135.83, 153.50 ($C^{25}O$), 155.30 (=CHN), 191.69 (C=O); **IR (ATR) ν_{max}(cm^{-1}):** 3420 (H_2O), 3053 (Ar–H), 2956 (CH_3), {1650, 1610, 1594, 1564 } (C=O, C=N, Ar), 1292, 1263 (C–O); **ESI-MS**: (*m*/*z*) 428.2 (M^{2+}/2); **Anal. Calcd for $C_{54}H_{60}Br_2N_6O_4\cdot 3H_2O$**: C, 60.56; H, 6.21; N, 7.85. Found: C, 60.30; H, 6.01; N, 7.84%.

4.2.5. 9,20-Bis{2-[3-(N-pyridinium-1-yl)propoxy]benzoyl}-7,18-dihydrodinaphtho[b,i][1,4,8,11]tetraazacyclotetradecine dibromide dihydrate ***7***. Pyridine (10 mL) was added to **3** (0.1 g, 0.11 mmol) and the mixture was stirred at 80 °C for 8 h. The solution was then cooled and left overnight in a refrigerator. Yellow crystalline product was collected, washed with diethyl ether, dried and chromatographed on a column with basic Al_2O_3. A mixture of dichloromethane–methanol (20:1) was used to separate less polar by-products, then the main yellow fraction of **7** was eluted with methanol, evaporated to dryness and recrystallized from the mixture methanol–dichloromethane (10:1) layered with *tert*-butyl methyl ether. Yellow crystals, yield 0.095 g (81%), mp 284–286 °C. **^{1}H NMR (300 MHz, DMSO-d_6, δ ppm):** 2.30 (m, 4H, CH_2^b), 4.20 (t, *J*=5.8 Hz, 4H, CH_2O), 4.64 (t, *J*=6.9 Hz, 4H, CH_2N^+), 7.18 (dd, *J*=7.4, 7.4 Hz, 2H, $H^{28,28'}$), 7.26 (d, *J*=8.4 Hz, 2H, $H^{26,26'}$), 7.46 (m, 6H, $H^{3,4,29,29',14,15}$), 7.59 (m, 2H, $H^{27,27'}$), 7.83 (s, 4H, $H^{1,6,12,17}$), 7.86 (m, 4H, $H^{2,5,13,16}$), 7.94 (dd, *J*=7.5, 7.6 Hz, 4H, $H^{e,e'}$), 8.49 (t, *J*=7.8 Hz, 2H, $H^{f,f'}$), 8.74 (d, *J*=6.2 Hz, 4H, N=C–H), 8.99 (b. d, *J*=6.1 Hz, 4H, $H^{d,d'}$), 13.58 (t, *J*=6.3 Hz, 2H, NH); **^{13}C NMR (75 MHz, DMSO-d_6, δ ppm):** 30.22 (CH_2), 58.22 (CH_2O), 65.07 (CH_2N^+), 110.30, 112.88, 113.09, 121.23, 126.20, 127.57, 127.85, 128.54, 129.58, 131.58, 131.86, 136.02, 144.63 (C^f), 145.44 (C^d), 153.43 ($C^{25}O$), 155.05 (=CHN), 191.42 (C=O); **IR (ATR) ν_{max}(cm^{-1}):** 3395 (H_2O), 3053 (Ar–H), 1650, 1607, 1593, 1560 } (C=O, C=N, Ar), 1290, 1261 (C–O); **ESI-MS**: (*m*/*z*) 434.2 (M^{2+}/2); **Anal. Calcd for $C_{56}H_{48}Br_2N_6O_4\cdot 2H_2O$:** C, 63.16; H, 4.92; N, 7.89. Found: C, 63.00; H, 4.94; N 7.82%.

4.2.6. 9,20-Bis[3-(N-pyridinium-1-yl)propyl]-7,18-dihydrodinaphtho[b,i][1,4,8,11]tetraazacyclotetradecine dibromide methanol disolvate ***9***. Pyridine (2 mL) was added to **5** (0.023 g, 0.04 mmol) and the mixture was stirred at 80 °C for 7 h. The solution was then cooled and left to crystallise in a refrigerator. Red precipitate was collected and recrystallized from methanol–diethyl ether (1:1). Red crystals, yield 0.02 g (59%), mp 252–254 °C. Crystals suitable for X-ray measurements were grown from methanol–diethyl ether. **^{1}H NMR (300 MHz, DMSO-d_6, δ ppm):** 2.32 (m, 4H, CH_2), 4.76 (t, *J*=7.3 Hz, 4H, CH_2N^+), 7.33 (m, 4H, Ar–H), 7.73 (m, 4H, Ar–H), 7.87 (s, 4H, $H^{1,6,12,17}$), 8.18 (dd, *J*=7.6, 7.6 Hz, 4H, $H^{b,b'}$), 8.30 (d, *J*=5.8 Hz, 4H,=CHN), 8.61 (tt, *J*=1.2, 7.8 Hz, 2H, $H^{c,c'}$), 9.21 (b d, *J*=5.8 Hz, 4H, $H^{a,a'}$), 12.74 (t, *J*=5.9 Hz, 2H, NH); **^{13}C NMR (75 MHz, DMSO-d_6, δ ppm):** 29.02 (CH_2), 32.97 (CH_2), 60.57 (CH_2N^+), 107.20, 110.17, 124.98, 126.89, 128.00, 131.07, 136.78, 144.87 (C^c), 145.42 (C^a), 148.70 (=CHN); **IR (ATR) ν_{max}(cm^{-1}):** 3356 (CH_3OH), 3122 (NH), 3053 (Ar–H), 2930 (CH_2), {1638, 1619, 1544 } (C=N, Ar); **ESI-MS:** (*m*/*z*) 314.1 (M^{2+}/2); **Anal. Calcd for $C_{42}H_{40}Br_2N_6\cdot 2CH_3OH$**: C, 61.98; H, 5.67; N, 9.86. Found: C 61.64; H, 5.55; N, 9.81%.

4.2.7. Lacunar compound ***10***. Compound **10** was isolated by careful chromatography of the reaction mixture containing **4**.[8] It was separated as a second yellow fraction using toluene–acetone (40:1) and additionally chromatographed on silica gel using methylene chloride-acetone (100:1). Pale-yellow microcrystalline product, yield 14%, mp>300 °C. The product contains non-stoichiometric amounts of acetone and methylene chloride, as judged from ^{1}H NMR spectrum. **^{1}H NMR (300 MHz, $CDCl_3$, δ ppm):** 1.56 (m, 4H, CH_2), 3.75 (sz. t, 4H, CH_2O), 6.80 (d, *J*=8.1 Hz, 2H, $H^{26,26'}$), 7.13 (ddd, *J*=7.5 Hz, *J*=7.5 Hz, *J*=0.8 Hz, 2H, $H^{28,28'}$), 7.42 (m, 6H, H $^{3,4,14,15,27,27'}$), 7.61 (s, 4H, $H^{1,6,12,17}$), 7.67 (dd, *J*=1.8 Hz, *J*=7.5 Hz, $H^{29,29'}$), 7.78 (m, 4H, $H^{2,5,13,16}$), 8.53 (d, *J*=6.4 Hz, 4H, N=C–H), 14.02 (t, *J*=6.4 Hz, 2H, NH); **^{13}C NMR (75 MHz, $CDCl_3$, δ ppm):** 26.23 (CH_2), 68.68 (CH_2O), 112.25, 114.31, 121.41, 126.05, 127.49, 129.42, 130.34, 132.16, 132.21, 138.63, 155.26 ($C^{25}O$), 156.31 (=CHN); **IR (ATR) ν_{max}(cm^{-1}):** 3055 (Ar–H), {2950, 2876 } (CH_2), 1651, 1584, 1557 } (C=O, C=N, Ar), {1287, 1259 } (C–O); **APCI-HRMS**: (*m*/*z*) 683.2642 ($M+H^+$), calcd 683.2658.

4.3. Crystallographic data

X-ray measurements for crystals **2** were performed on SuperNova diffractometer (Agilent Technologies)[18]—equipped with Dual Mo or Cu at zero Atlas measurement device and CryoJet low temperature device—using CuKα (λ=1.54184 Å); data collection: CrysAlisPRO;[18] cell refinement: CrysAlisPRO;[18] data reduction: CrysAlisPRO;[18] absorption correction: multi-scan.[18] Program used to solve structure: SIR92;[19] program used to refine structure: SHELXL97;[20] molecular graphics: ORTEP-3;[21] software used to prepare material for publication: SHELXL97[20] and WinGX.[22]

X-ray diffraction data for crystal **9** were collected at 100 K by the ω-scan technique using a Bruker AXS Smart APEX-II CCD diffractometer with MonoCap capillary and monochromated Cu-K_α radiation (λ=1.54178 Å). Data collection, cell refinement, data reduction, analysis and absorption correction were carried out with the SMART and SAINT-PLUS;[23] molecular graphics: Mercury CSD;[24]

software used to prepare material for publication: SHELXL2014[20] and Platon.[25] The structure was solved by direct methods with SHELXS[20] and refined by a full-matrix least-squares technique on F^2 using SHELXL2014[20] with anisotropic thermal parameters for the non-H atoms.

The structures were solved by direct methods and refined by full matrix least squares on F^2 using anisotropic displacement parameters for non-hydrogen atoms. The hydrogen atoms of aromatic C–H, methylene and methine groups were found on Fourier difference maps and included in the refinement in the positions calculated from geometrical conditions. The hydrogen atoms at N and *O*-atoms were localized on Fourier difference maps and refined with restrained N–H and O–H distances (DFIX procedure in SHELXL97) in riding model with $U_{iso}=U_{eq}$ of parent atom. The crystal data and refinement parameters are listed in Table S1.

Crystal data: **2** $C_{32}H_{32}N_4O_2$: T=120.0(1)K, monoclinic, space group $P2_1/n$, a=4.8827(1), b=20.4455(4), c=12.3580(2) Å, β=90.082(2)°, V=1233.69(4)Å^3, Z=2, Dx=1.358 Mg m^{-3}. Intensity data: θ_{max}=76.96°, completeness 99.6%, R=0.0352 for 2422 reflections with I>2σ(I), wR2=0.0992 for all 2593 unique reflections; Goodness-of-fit parameters S=0.994. CCDC No. 1043396.

Crystal data: **9** $(C_{42}H_{40}N_6)^{2+}\cdots 2Br^-\cdots 2CH_3OH$: T=100.0(1) K, monoclinic, space group $P2_1/c$, a=10.1532(3), b=15.7907 (5), c=13.2346 (4) Å, β=112.1249(10)°, V=1965.62(10) Å^3, Z=2, Dx=1.441 Mg m^{-3}. Intensity data: θ_{max}=67.0°, completeness 99.0%, R=0.0497 for 3505 reflections with I>2σ(I), wR2=0.1328 for all 3505 unique reflections, Goodness-of-fit parameter S=1.084. CCDC No. 1042368.

4.4. UV–vis spectroscopy and quantum chemical calculations

Quantum chemical calculations reported in this work were performed using Gaussian 09 rev. A.02 software.[26] Geometries of all compounds **6**–**9** were optimized using Density Functional Theory methodology with B3LYP functional and the 6–31+G** basis set. Polarizable Continuum Model (PCM) approach with default Gaussian 09 parameters for water was used to account for the solvent. Crystallographic data available for compounds **8** and **9** were used as starting structures in geometry optimization of these molecules. Initial structures for other molecules were based on the conformation of macrocyclic core of **8**. Energies of electronic transitions for optimized structures compounds 6–9 were calculated within Time Dependent DFT approach at the B3LYP/6–31+G** level with water treated as implicit PCM solvent.

4.5. Spectrophotometric studies and DNA binding

The electronic absorption spectra were obtained on Varian Cary 100 Bio spectrometer, CD spectra on JASCO J815 spectrophotometer and fluorescence spectra on the Varian Eclipse fluorimeter, all in quartz cuvettes (1 cm). The spectroscopic studies were performed in aqueous buffer solution (pH=7, sodium cacodylate buffer, I=0.05 mol dm^{-3}). Under the experimental conditions absorbance of **8** was proportional to its concentration. Polynucleotides were purchased as noted: poly dAdT–poly dAdT, poly dGdC–poly dGdC (Sigma), calf thymus (*ct*)-DNA (Aldrich). Polynucleotides were dissolved sodium cacodylate buffer, I=0.05 mol dm^{-3}, pH=7. Calf thymus (*ct*-) DNA was additionally sonicated and filtered through a 0.45 μm filter.[27,28] Polynucleotide concentration was determined spectroscopically[27] as the concentration of phosphates. Spectroscopic titrations were performed by adding portions of polynucleotide solution into the solution of the studied compound.

Obtained data were corrected for dilution. Titration data were processed by Scatchard equation.[14] Values for K_s and n given in Table 2 all have satisfactory correlation coefficients (>0.99). Thermal melting curves for DNA, RNA and their complexes with studied compounds were determined as previously described[28,29] by following the absorption change at 260 nm as a function of temperature. Absorbance of the ligands was subtracted from every curve, and the absorbance scale was normalized. The T_m values are the midpoints of the transition curves, determined from the maximum of the first derivative and checked graphically by the tangent method.[28] ΔT_m values were calculated subtracting T_m of the free nucleic acid from T_m of the complex. Every ΔT_m value here reported was the average of at least two measurements, the error in ΔT_m is±0.5 °C.

Acknowledgements

This research was performed using equipment purchased thanks to the financial support of the European Regional Development Fund in the framework of the Polish Innovation Economy Operational Program (contract no. POIG.02.01.00-12-023/08). I.P. et al. acknowledge the financial support of the Croatian Science Foundation (grant No. 1477) and FP7-REGPOT-2012-2013-1, Grant Agreement Number 316289–InnoMol.

Supplementary data

Supplementary data (crystallographic details for **2** and **9**, APCI-MS, ^{1}H NMR and ROESY spectra of **10**, detailed data of DNA binding experiments) related to this article can be found at http://dx.doi.org/10.1016/j.tet.2015.04.098.

References and notes

1. (a) Fiel, R. J.; Howard, J. C.; Mark, E. H.; Datta-Gupta, N. *Nucleic Acids Res.* **1979**, *6*, 3093; (b) Pasternack, R. F.; Gibs, E. J.; Villafranca, J. J. *Biochemistry* **1983**, *22*, 2406; (c) Fiel, R. J. *J. Biomol. Struct. Dyn.* **1989**, *6*, 1259; (d) Johnson, D. S.; Boger, D. L. In *Comprehensive Supramolecular Chemistry*; Atwood, J. L., Davies, J. E. D., MacNicol, D. D., Vögtle, F., Eds.; Pergamon: Oxford, New York, NY, 1996; Vol. 4, Chapter 3, pp 73–176; and references cited therein; (e) McMillin, D. R.; McNett, K. M. *Chem. Rev.* **1998**, *98*, 1201; (f) Armitage, B. *Chem. Rev.* **1998**, *98*, 1171; (g) Bailly, C. *Curr. Med. Chem.* **2000**, *7*, 39; (h) Pasternack, R. F.; Ewen, S.; Rao, A.; Meyer, A. S.; Freedman, M. A.; Collings, P. J.; Frey, S. L.; Ranen, M. C.; de Paula, J. C. *Inorg. Chim. Acta.* **2001**, *317*, 59; (i) *DNA and RNA Binders*; Demeunynck, M., Bailly, C., Wilson, W. D., Eds.; Wiley-VCH: Weinheim, 2003; (j) McMillin, D. R.; Shelton, A. H.; Bejune, S. A.; Fanwick, P. E.; Wall, R. K. *Coord. Chem. Rev.* **2005**, *249*, 1451; (k) Martinez, R.; Chacon-Garcia, L. *Curr. Med. Chem.* **2005**, *12*, 127; (l) Zeglis, B. M.; Pierre, V. C.; Barton, J. K. *Chem. Commun.* **2007**, 4565; (m) Hannon, M. J. *Chem. Soc. Rev.* **2007**, *36*, 280.
2. (a) Fiel, R. J.; Gupta, N. D.; Mark, E. H.; Howard, J. C. *Cancer Res.* **1981**, *41*, 354; (b) Dixon, D. W.; Schinazi, R.; Marzilli, L. G. *Ann. N. Y. Acad. Sci.* **1990**, *616*, 511; (c) Wheelhous, R. T.; Sun, D.; Han, F. X.; Hurly, L. H. *J. Am. Chem. Soc.* **1998**, *120*, 3261; (d) Izbicka, E.; Wheelhouse, R. T.; Raymond, E.; Davidson, K. K.; Lawrence, R. A.; Sun, D.; Windle, B. E.; Hurley, L. H.; Hoff, D. D. V. *Cancer Res.* **1999**, *59*, 639; (e) Priola, S. A.; Raines, A.; Caughey, W. S. *Science* **2000**, *287*, 1503; (f) Woodburn, K. W.; Phillips Bellinger, G. C. A.; Sadek, M.; Brownlee, R. T. C.; Reiss, J. M. *Bioorg. Med. Chem. Lett.* **1992**, *2*, 343; (g) Tronconi, M.; Colombo, A.; De Cesare, M.; Marchesini, R.; Woodburn, K. W.; Reiss, J. A.; Phillips, D. R.; Zunino, F. *Cancer Lett.* **1995**, *88*, 41; (h) Van Vliet, L. D.; Ellis, T.; Foley, P. J.; Liu, L.; Pfeffer, F. M.; Russell, R. A.; Warrener, R. N.; Hollfelder, F.; Waring, M. J. *J. Med. Chem.* **2007**, *50*, 2326; (i) Xue, L.; Xi, H.; Kumar, S.; Gray, D.; Davis, E.; Hamilton, P.; Skriba, M.; Arya, D. P. *Biochemistry* **2010**, *49*, 5540; (j) Samanta, S. K.; Dutta, D.; Roy, S.; Bhattacharya, K.; Sarkar, S.; Dasgupta, A. K.; Pal, B. C.; Mandal, C.; Mandal, C. *J. Med. Chem.* **2013**, *56*, 5709; (k) Rahman, K. M.; Jackson, P. J. M.; James, C. H.; Basu, B. P.; Hartley, J. A.; de la Fuente, M.; Schatzlein, A.; Robson, M.; Pedley, R. B.; Pepper, C.; Fox, K. R.; Howard, P. W.; Thurston, D. E. *J. Med. Chem.* **2013**, *56*, 2911.
3. (a) Basato, M.; Corain, B.; Favero, G.; Valle, G.; Eilmes, J. *Inorg. Chim. Acta* **1989**, *159*, 59; (b) Eilmes, J. *Polyhedron* **1992**, *11*, 581; (c) Eilmes, J.; Ptaszek, M.; Woźniak, K. *Polyhedron* **2002**, *21*, 7; (d) Grolik, J.; Zwoliński, K.; Sieroń, L.; Eilmes, J. *Tetrahedron* **2011**, *67*, 2623; (e) Grolik, J.; Dudek, Ł.; Eilmes, J.; Eilmes, A.; Górecki, M.; Frelek, J.; Heinrich, B.; Donnio, B. *Tetrahedron* **2012**, *68*, 3875.
4. (a) Pawlica, D.; Radić-Stojković, M.; Sieroń, L.; Piantanida, I.; Eilmes, J. *Tetrahedron* **2006**, *62*, 9156; (b) Radić-Stojković, M.; Piantanida, I.; Kralj, M.; Marjanović, M.; Žinić, M.; Pawlica, D.; Eilmes, J. *Bioorg. Med. Chem.* **2007**, *15*, 1795; (c) Pawlica, D.; Radić-Stojković, M.; Dudek, Ł.; Piantanida, I.; Sieroń, L.; Eilmes, J. *Tetrahedron* **2009**, *65*, 3980; (d) Radić-Stojković, M.; Marjanović, M.; Pawlica, D.; Dudek, Ł.; Eilmes, J.; Kralj, M.; Piantanida, I. *New J. Chem.* **2010**, *34*, 500.
5. Radić-Stojković, M.; Škugor, M.; Tomić, S.; Grabar, M.; Smrečki, V.; Dudek, Ł.; Grolik, J.; Eilmes, J.; Piantanida, I. *Org. Biomol. Chem.* **2013**, *11*, 4077.

6. (a) Hunter, C. A.; Sanders, J. K. M. *J. Am. Chem. Soc.* **1990**, *112*, 5525; (b) Schneider, H.-J.; Wang, M. *J. Org. Chem.* **1994**, *59*, 7464; (c) Schneider, H.-J.; Sartorius. *J. Chem. Soc., Perkin Trans. 2* **1997**, 2319.
7. (a) Friedman, A. E.; Chambron, J.-C.; Sauvage, J.-P.; Turro, N. J.; Barton, J. K. *J. Am. Chem. Soc.* **1990**, *112*, 4960; (b) Jenkins, Y.; Friedman, A. E.; Turro, N. J.; Barton, J. K. *Biochemistry* **1992**, *31*, 10809; (c) Hiort, C.; Lincoln, P.; Nordén, B. *J. Am. Chem. Soc.* **1993**, *115*, 3448; (d) Turro, C.; Bossmann, S. H.; Jenkins, Y.; Barton, J. K.; Turro, N. J. *J. Am. Chem. Soc.* **1995**, *117*, 9026; (e) Olson, E. J. C.; Hu, D.; Hormann, A.; Jonkman, A. M.; Arkin, M. R.; Stemp, E. D. A.; Barton, J. K.; Barbara, P. F. *J. Am. Chem. Soc.* **1997**, *119*, 11458; (f) Tuite, E.; Lincoln, P.; Nordén, B. *J. Am. Chem. Soc.* **1997**, *119*, 239; (g) Yam, V. W. W.; Lo, K. K. W.; Cheung, K. K.; Kong, R. Y. C. *J. Chem. Soc., Dalton Trans.* **1997**, 2067; (h) Holmlin, R. E.; Stemp, E. D. A.; Barton, J. K. *Inorg. Chem.* **1998**, *37*, 29; (i) Che, C.-M.; Yang, M.; Wong, K. H.; Chan, H.-L.; Lam, W. *Chem. Eur. J.* **1999**, *5*, 3350; (j) Erkkila, K. E.; Odom, D. T.; Barton, J. K. *Chem. Rev.* **1999**, *99*, 2777; (k) Ruba, E.; Hart, J. R.; Barton, J. K. *Inorg. Chem.* **2004**, *43*, 4570; (l) Hart, J. R.; Johnson, M. D.; Barton, J. K. *Proc. Natl. Acad. Sci. U.S.A.* **2004**, *101*, 14040; (m) Zeglis, B. M.; Barton, J. K. *J. Am. Chem. Soc.* **2006**, *128*, 5654.
8. Kaźmierska, A.; Gryl, M.; Stadnicka, K.; Eilmes, J. *Supramol. Chem.* **2013**, *5*, 276.
9. Hanke, R.; Breitmaier, E. *Chem. Ber.* **1982**, 1657.
10. Appel, R. *Angew. Chem., Int. Ed. Engl.* **1975**, *14*, 801.
11. Grolik, J.; Dominiak, P. M.; Sieroń, L.; Woźniak, K.; Eilmes, J. *Tetrahedron* **2008**, *64*, 7796.
12. *The Weak Hydrogen Bond in Structural Chemistry and Biology*; Desiraju, G. R., Steiner, T., Eds.; Oxford University: New York, NY, 2001.
13. Martin, R. L. *J. Chem. Phys.* **2003**, *118*, 4775.
14. (a) Scatchard, G. *Ann. N. Y. Acad. Sci.* **1949**, *51*, 660; (b) McGhee, J. D.; von Hippel, P. H. *J. Mol. Biol.* **1976**, *103*, 679.
15. *Circular Dichroism Principles and Applications*; Berova, N., Nakanishi, K., Woody, R. W., Eds.; Wiley-VCH: New York, NY, 2000.
16. *Circular Dichroism and Linear Dichroism*; Rodger, A., Norden, B., Eds.; Oxford University: New York, NY, 1997, Chapter 2.
17. Cantor, C. R.; Schimmel, P. R. Biophysical Chemistry In; WH Freeman: San Francisco, CA, 1980; pp 1109–1181.
18. SuperNova™, CrysAlis Software System, v. 1.171; Agilent Technologies: Yarnton, England 2011.
19. Altomare, A.; Cascarano, G.; Giacovazzo, C.; Guagliardi, A.; Burla, M. C.; Polidori, G.; Camalli, M. *J. Appl. Crystallogr.* **1994**, *27*, 435.
20. Sheldrick, G. M. *Acta Crystallogr.* **2008**, *A64*, 112.
21. Farrugia, L. J. *J. Appl. Crystallogr.* **1997**, *30*, 565.
22. Farrugia, L. J. *J. Appl. Crystallogr.* **1999**, *32*, 837.
23. SMART and SAINT-PLUS, Bruker (2013). Bruker AXS., Madison, Wisconsin, USA.
24. Macrae, C. F.; Bruno, I. J.; Chisholm, J. A.; Edgington, P. R.; McCabe, P.; Pidcock, E.; Rodriguez-Monge, L.; Taylor, R.; van de Streek, J.; Wood, P. A. *J. Appl. Crystallogr.* **2008**, *41*, 466.
25. Spek, A. L. *Acta Crystallogr.* **2009**, *D65*, 148.
26. Frisch, M. J.; Trucks, G. W.; Schlegel, H. B.; Scuseria, G. E.; Robb, M. A.; Cheeseman, J. R.; Scalmani, G.; Barone, V.; Mennucci, B.; Petersson, G. A.; Nakatsuji, H.; Caricato, M.; Li, X.; Hratchian, H. P.; Izmaylov, A. F.; Bloino, J.; Zheng, G.; Sonnenberg, J. L.; Hada, M.; Ehara, M.; Toyota, K.; Fukuda, R.; Hasegawa, J.; Ishida, M.; Nakajima, T.; Honda, Y.; Kitao, O.; Nakai, H.; Vreven, T.; Montgomery, J. A., Jr.; Peralta, J. E.; Ogliaro, F.; Bearpark, M.; Heyd, J. J.; Brothers, E.; Kudin, K. N.; Staroverov, V. N.; Kobayashi, R.; Normand, J.; Raghavachari, K.; Rendell, A.; Burant, J. C.; Iyengar, S. S.; Tomasi, J.; Cossi, M.; Rega, N.; Millam, J. M.; Klene, M.; Knox, J. E.; Cross, J. B.; Bakken, V.; Adamo, C.; Jaramillo, J.; Gomperts, R.; Stratmann, R. E.; Yazyev, O.; Austin, A. J.; Cammi, R.; Pomelli, C.; Ochterski, J. W.; Martin, R. L.; Morokuma, K.; Zakrzewski, V. G.; Voth, G. A.; Salvador, P.; Dannenberg, J. J.; Dapprich, S.; Daniels, A. D.; Farkas, Ö.; Foresman, J. B.; Ortiz, J. V.; Cioslowski, J.; Fox, D. J. *Gaussian 09, Rev. A.02*; Gaussian,: Wallingford CT, 2009.
27. Chaires, J. B.; Dattagupta, N.; Crothers, D. M. *Biochemistry* **1982**, *21*, 3933.
28. Piantanida, I.; Palm, B. S.; Čudić, P.; Žinić, M.; Schneider, H.-J. *Tetrahedron* **2004**, *60*, 6225.
29. Mergny, J.-L.; Lacroix, L. *Oligonucl.* **2003**, *13*, 515.